Hydrology and Water Resources
https://www.sciltp.com/journals/hwr

Article

Physical Interpretation of the Complementary Relationship for Evapotranspiration

Sha Zhou [1,2,*] and Bofu Yu [3]

[1] State Key Laboratory of Earth Surface Processes and Disaster Risk Reduction, Faculty of Geographical Science, Beijing Normal University, Beijing 100875, China
[2] Institute of Land Surface System and Sustainable Development, Faculty of Geographical Science, Beijing Normal University, Beijing 100875, China
[3] School of Engineering and Built Environment, Griffith University, Nathan, QLD 4111, Australia
* Correspondence: shazhou21@bnu.edu.cn

How To Cite: Zhou, S.; Yu, B. Physical Interpretation of the Complementary Relationship for Evapotranspiration. *Hydrology and Water Resources* **2026**, *1*(1), 6. https://doi.org/10.53941/hwr.2026.100006

Received: 16 November 2025
Revised: 8 January 2026
Accepted: 19 January 2026
Published: 2 February 2026

Abstract: The complementary relationship (CR) between actual evapotranspiration (ET) and apparent potential evapotranspiration (PET_a) is widely adopted as a simple yet powerful approach for ET estimation over land. However, most existing CR formulations remain empirical, largely due to a lack of clear physical interpretation of its key parameter. In this study, we show that the CR naturally emerges from the surface energy balance and clarify the physical meaning of its parameter: the wet Bowen ratio, defined as the Bowen ratio when the surface becomes saturated. Fundamentally, the CR originates from the partitioning of available energy: ET is directly linked to the latent heat flux, while PET_a is proportional to the sensible heat flux. Additionally, the CR can be interpreted as the atmospheric response (encapsulated by PET_a) to ET dynamics across wet and dry conditions. In contrast, ET exhibits a positive relationship with the energy-based potential evapotranspiration (PET_e), which controls and drives ET over land. This physically grounded relationship among ET, PET_a, and PET_e advances our understanding of the spatial and temporal variations in ET, as well as its critical role in land-atmosphere interactions, thereby facilitating the practical application of the CR for ET estimation across diverse environments.

Keywords: Evapotranspiration, complementary relationship, surface energy partitioning, Bowen ratio

1. Introduction

Terrestrial evapotranspiration (ET) is critical to land-atmosphere exchanges of water, energy, and carbon fluxes and serves as a key nexus linking hydrological, ecological, and climate systems, with profound implications for water resource management, agricultural productivity, and climate change projections [1–4]. However, both direct observation and indirect estimation of ET remain challenging and highly uncertain [5–7]. This uncertainty primarily arises from the complex interactions of soil moisture dynamics, vegetation physiological traits (e.g., stomatal conductance) and structural characteristics (e.g., leaf area index, canopy architecture)—coupled with the inherent challenges of parameterizing these complex land surface processes [8–10]. To address this complexity, the complementary relationship (CR) for ET, first proposed by Bouchet [11] and operationalized by Morton [12], offers a simple conceptual framework for ET estimation. Its core advantage is that it relies solely on routine meteorological observations and requires no detailed knowledge of land surface properties, making it highly practical for large-scale applications or regions with limited land surface data by indirectly inferring ET dynamics from readily available atmospheric variables [13–16].

The CR essentially describes the relationship between three types of ET over land surface [17]. The first type is the actual ET, which is the water vapor flux from open water, wet soil and vegetation over an area. The second type is the potential ET (PET), i.e., the ET that would occur from the same area with the same net radiation, but with unlimited water supply, i.e., a saturated evaporative surface. As the PET is limited by available energy, it is termed as PET_e in this study. The third type is the apparent potential ET (PET_a), which is the ET that would occur from a small, saturated surface within a large and unsaturated area, with abundant energy supply from the net radiation and the surrounding environment [18]. It is assumed that the saturated evaporative surface is too small to affect aerodynamic conditions, i.e., air temperature, humidity, and wind speed. PET_a therefore depends on the prevailing aerodynamic conditions over the large dry area. In practice, PET_e is represented by the actual ET over a large lake or reservoir, while PET_a by the actual ET measured with an evaporation pan placed in an otherwise dry environment [19]. These three types of ET converge when the large area is saturated everywhere. As the large area dries up, ET is limited by available water and falls below PET_e. Simultaneously, a lower ET reduces the moisture content of the atmosphere and reduced evaporative cooling increases air temperature, resulting in a warmer and drier atmosphere with a higher PET_a than PET_e. These processes lead to a complementary relationship between ET and PET_a when water supply is limited.

Based on the conceptual framework above, a series of CR formulations have been developed [11,17,20–27] and applied to large-scale ET estimation [14–16,28–30]. However, most CR formulations remain empirical due to a lack of physical interpretation of parameters involved in CR formulations [13]. These parameters thus require calibration using site-specific observations, which limits their broader application in ET estimation. Calibration-free CR formulations [15,25,27] essentially rely on an assumed non-linear relationship between ET, PET_e, and PET_a, yet the intrinsic mechanisms driving the hypothesized non-linearity remain unclear [17,23,26]. Additionally, the absence of definitive methods for estimating PET_e and PET_a further hinders development of physically-based, calibration-free CR formulations. Previous studies generally use the Priestley-Taylor equation [31] to approximate PET_e, and pan evaporation or the Penman equation [32] to approximate PET_a. However, these estimates do not align with the strict definitions of PET_e and PET_a [18,23,27]. An in-depth understanding of the physical processes underlying the complementary relationship, coupled with accurate estimation of PET_e and PET_a, is therefore crucial for developing a physically sound CR formulation.

Zhou and Yu [33] disentangled the original Penman equation into an energy-based PET (PET_e) and an aerodynamics-based PET (PET_a). They further established a theoretical relationship between ET, PET_e, and PET_a based on land-atmosphere interactions [33]. This theoretical relationship closely resembles the CR framework, yet it remains unclear whether the proposed methods for estimating PET_e and PET_a—along with their distinct relationships with ET—align with the core concept and mechanism of the CR framework. Nevertheless, this work offers a fresh perspective for revisiting the CR framework and advancing our understanding of its underlying physical processes.

The aim of this study is to formulate a physically-based CR and gain a deeper insight into its mechanistic foundations. We first revisit the core concepts of the CR framework and outline the practical challenges associated with the existing CR formulations. Leveraging energy-based and aerodynamics-based approaches to estimate PET_e and PET_a, respectively, we demonstrate that a CR with a parameter of clear physical meaning naturally emerges from the surface energy balance. We further show the consistency of this physically-based CR with the theoretical relationship derived from land-atmosphere interactions [33]. This work advances our understanding of the CR's underlying physical processes, i.e., the surface energy balance and land-atmosphere interactions, thereby supporting its practical application for ET estimation over land.

2. Concept of the Complementary Relationship

When the land surface is adequately supplied with water (moisture-unlimited conditions), the three key ET terms are equal in magnitude (i.e., representing wet-surface evaporation):

$$ET = PET_e = PET_a \tag{1}$$

The magnitude of these terms is determined solely by energy supply and aerodynamic conditions.

As surface moisture supply decreases, available water becomes insufficient to meet the atmospheric evaporative demand, i.e., PET_e. The energy that would otherwise be consumed by ET is redirected to sensible heat flux (H), resulting in a drier and warmer atmosphere. This atmospheric adjustment causes PET_a, defined as the evaporation from an arbitrarily small, wet area (e.g., an evaporation pan) within a dry environment, to exceed PET_e. For moisture-limited conditions, we have

$$ET < PET_e < PET_a \tag{2}$$

The original CR proposed by Bouchet [11] assumes symmetry between the decrease in ET and the increase in PET_a, relative to the wet-surface evaporation (PET_e), from wet to dry conditions.

$$PET_e - ET = PET_a - PET_e \quad (3)$$

This symmetry is predicated on the assumption of constant available energy (i.e., net radiation minus ground heat flux) between wet and dry conditions. Under this premise, the decrease in latent heat flux equals the increase in sensible heat flux, i.e., $\lambda PET_e - \lambda ET = H - H_w$, where λ is the latent heat of vaporization and H_w the sensible heat flux under wet conditions. In reality, variations in energy transfer processes (e.g., the relationship between changes in H and λPET_a) may deviate from strict symmetry. Thus, it is more realistic to assume a proportional relationship between the left and right hand-sides of Equation (3) [22], resulting in a generalized linear CR:

$$PET_e - ET = k(PET_a - PET_e) \quad (4)$$

Rearranging Equation (4) yields an explicit expression for ET:

$$ET = (1 + k)PET_e - kPET_a \quad (5)$$

where k is the coefficient of proportionality, and it can be interpreted as a measure of asymmetry for CR. When $k = 1$, Equations (4) and (5) are reduced to Bouchet's original symmetric CR, i.e., Equation (3). For $k \neq 1$, the CR becomes asymmetric—a characteristic widely noted and validated with observational evidence [19,22,24,34]. This asymmetry primarily arises from additional energy inputs to the small wet surface (e.g., evaporation pans) from the surrounding environment, such as lateral/bottom heat transfer and local energy advection. These processes cause PET_a to increase more substantially than the corresponding decrease in ET, leading to $k < 1$ in most practical scenarios [19,24]. Given the uncertainty in energy transfer from the surrounding environment, pan evaporation rates are highly sensitive to pan characteristics (e.g., size, material, and exposure), rendering PET_a inherently indeterminate and uncertain in practice.

Building on the above conceptual framework of CR, its distinct characteristics can be outlined as follows: (1) a fundamental assumption of constant available energy between wet and dry conditions; (2) two boundary conditions (Equations (1) and (2)) that constrain the quantitative relationships between ET, PET_e, and PET_a under wet and dry conditions; (3) physical basis for the complementary relationship between ET and PET_a originates from the shift in surface energy partitioning (latent vs. sensible heat flux) and associated land-atmosphere feedbacks as surface moisture changes.

The generalized form (Equation (5)) unifies most existing CR formulations, with the corresponding k values for different formulations summarized in Table 1. Despite its generality, existing CR formulations face notable practical limitations. First, uncertainties in the estimation of PET_e and PET_a often violate the boundary conditions, i.e., Equations (1) and (2). PET_e is commonly estimated using the Priestley-Taylor equation [31]. However, this empirical method yields results that diverge substantially from observed oceanic ET, indicating its inability to adequately quantify wet-surface evaporation [18,35,36]. PET_a is typically measured via an evaporation pan or estimated using the Penman equation [32]. However, pan evaporation rates are inherently uncertain in practical applications: they are highly sensitive to pan characteristics, and the Class A evaporation pan, being sufficiently large, alters air temperature and humidity around the pan, which does not conform with the definition of PET_a. Furthermore, PET_a derived from the original Penman equation or its variants tends to be underestimated because the equation neglects energy transfer from the surrounding environment [18]. Second, the physical interpretation and quantitative derivation of k remain inconsistent across different formulations (Table 1). These uncertainties hinder the reliable application of CR for ET estimation in diverse climatic and surface conditions. In the following section, we demonstrate how these uncertainties can be minimalized by accurately estimating PET_e and PET_a in accordance with their definitions and boundary conditions, while clarifying the physical meaning of the coefficient of proportionality, k.

Table 1. The coefficient of proportionality (k) and its interpretation for different CR formulations.

CR Formulation	Coefficient of Proportionality (k)	Interpretation of k	References
$ET = 2PET_e - PET_a$	$k = 1$	Asymmetric, physically unrealistic	[11]
$ET = \left(1 + \frac{1}{b}\right)PET_e - \frac{1}{b}PET_a$	$k = \frac{1}{b}$	An empirical site-specific, fitted parameter	[20]
$ET = \left(1 + \frac{\gamma}{\Delta}\right)PET_e - \frac{\gamma}{\Delta}PET_a$	$k = \frac{\gamma}{\Delta}$	A special case with limited general applicability	[21,22]

Table 1. *Cont.*

CR Formulation	Coefficient of Proportionality (k)	Interpretation of k	References
$ET = \left(\frac{PET_e}{PET_a}\right)^2 (2PET_e - PET_a)$	$k \approx 0.22$	A special case with limited general applicability	[17]
$ET = \left(1 + \frac{X_{min}}{1 - X_{min}}\right) PET_e - \frac{X_{min}}{1 - X_{min}} PET_a$	$k = \frac{X_{min}}{1 - X_{min}}$	An empirical site-specific, fitted parameter	[23]
$ET = (1 + \beta_w)PET_e - \beta_w PET_a$	$k = \beta_w$	Physically meaningful and applicable across varying conditions	This study

3. Derivation and Validation of a Physically-Based Complementary Relationship

Here we show that the complementary relationship naturally emerges from the surface energy balance through clear definition and robust estimation of PET_e for fully saturated conditions and PET_a from a small, saturated surface in an otherwise dry environment, respectively.

3.1. Definition and Estimation of PET$_e$ and PET$_a$

PET_e represents the rate of ET that would occur when water supply is unlimited at the evaporative surface (i.e., the entire surface is fully saturated). PET_e cannot be directly measured unless the entire surface is saturated and must be estimated, typically using observations from dry conditions. Among available methods, the energy-based approach is deemed the most reliable for PET_e estimation [18],

$$\lambda PET_e = \frac{R_n}{1 + \beta_w} \tag{6}$$

where R_n ($J \cdot m^{-2} \cdot s^{-1}$) is the available energy (i.e., net radiation minus ground heat flux) and equals the sum of latent and sensible heat fluxes; β_w is the wet Bowen ratio, i.e., the ratio of sensible over latent heat fluxes when the evaporative surface is saturated.

PET_a represents the ET rate from a small, saturated surface (e.g., a tiny evaporation pan placed in a desert) within a larger, unsaturated surrounding area. The saturated area is assumed to be sufficiently small that its presence has no practical effect on the surrounding dry environment, ensuring identical prevailing meteorological condition over the small, wet area and the larger dry area. In this context, the energy available for evaporation at the small saturated surface originates from two sources: net radiation at the surface and heat advection from the surrounding dry environment. This dual energy input renders PET_a inherently indeterminate and uncertain if not constrained by additional assumptions. To address this challenge, we estimate the upper limit of PET_a by assuming that the surface temperature of the small, saturated area approximates its maximum value, i.e., the surface temperature of the surrounding dry area (T_s). Under this assumption, PET_a can be quantified using the aerodynamics-based approach:

$$\lambda PET_a = \frac{\rho c_p (e_s^* - e_a)}{\gamma r_a} \tag{7}$$

where ρ is the air density ($kg \cdot m^{-3}$), c_p the specific heat of air at constant pressure ($J \cdot kg^{-1} \cdot K^{-1}$), γ the psychrometric constant ($Pa \cdot K^{-1}$), r_a the aerodynamic resistance ($s \cdot m^{-1}$) that depends on wind speed and land surface characteristics, and the term $e_s^* - e_a$ is the difference in vapor pressure (Pa) between the saturated evaporative surface and the air above.

The assumption of equivalent surface temperature (T_s) implies that the sensible heat flux (H) of the small, saturated area is maximized and equal to that of the surrounding large dry area. Thus, PET_a can also be directly estimated as the ratio of H to the wet Bowen ratio (β_w) of the small, saturated area:

$$\lambda PET_a = \frac{H}{\beta_w} \tag{8}$$

$$\beta_w = \frac{\gamma (T_s - T_a)}{e_s^* - e_a} \tag{9}$$

where $T_s - T_a$ is the difference between surface (T_s) and air (T_a) temperatures (K). Previous studies have validated that β_w estimated from surface temperature (T_s) and meteorological variables (T_a and e_a) of the large dry area (consistent with those of the small wet area) remains relatively constant when the entire surface is saturated [18,33].

This constancy arises from the coupled changes in temperature and humidity at the evaporative surface and of the overlying air. Consequently, β_w derived from Equation (9) is applicable to both PET_a estimation (Equation (8)) and PET_e estimation (Equation (6)).

The energy-based PET_e estimation relies on two core assumptions: (1) constant available energy (R_n) under both wet and dry surface conditions; (2) constant wet Bowen ratio (β_w) for both the small, saturated area and the large area when fully saturated. The first assumption is widely adopted in PET_e estimation and aligns with the fundamental assumption of the CR framework. The second assumption has been rigorously validated in prior work [18,33] and addresses the critical limitation of the widely used Priestley-Taylor equation. Specifically, the implicit wet Bowen ratio in the Priestley-Taylor equation is highly sensitive to temperature variations between wet and dry conditions, leading to systematic biases in PET_e estimation [18,33,37]. This critical issue is resolved by invoking the constancy of β_w regardless of surface moisture changes, enabling accurate estimation of the wet Bowen ratio using readily available surface temperature observations and routine meteorological data.

3.2. Derivation of the Complementary Relationship

For a given large area, the surface energy balance equation is expressed as

$$R_n = \lambda ET + H \tag{10}$$

where the available energy, R_n, imposes a constraint on PET_e and the sensible heat flux, H, is directly related to PET_a. With R_n from Equation (6) and H from Equation (8), the energy balance equation can be re-written as:

$$ET = (1 + \beta_w)PET_e - \beta_w PET_a \tag{11}$$

The structural consistency between Equations (5) and (11) confirms that the coefficient of proportionality k equals the wet Bowen ratio β_w, i.e., $k = \beta_w$. This derivation also aligns with the boundary conditions of the CR framework: $ET = PET_e = PET_a$ for saturated surfaces (Equation (1)) and $ET < PET_e < PET_a$ for unsaturated surfaces (Equation (2)). Given that the partitioning of available energy (R_n) into latent heat flux (λET) and sensible flux (H) is governed by the actual Bowen ratio (β), defined as $\beta = H/\lambda ET$, the key relationships among ET, PET_e, and PET_a, all of which depend on this energy partitioning mechanism, are summarized in Table 2. These relationships demonstrate that the relative magnitudes of ET, PET_e, and PET_a are determined by surface wetness, as quantified by the difference between β and β_w.

Table 2. Estimation of the three types of ET and their relationships.

Equation	Range
$\lambda ET = \frac{R_n}{1+\beta}$	$\left[0, \frac{R_n}{1+\beta_w}\right]$
$\lambda PET_e = \frac{R_n}{1+\beta_w}$	$\frac{R_n}{1+\beta_w}$
$\lambda PET_a = \frac{H}{\beta_w}$	$\left[\frac{R_n}{1+\beta_w}, \frac{R_n}{\beta_w}\right]$
$\frac{ET}{PET_e} = \frac{1+\beta_w}{1+\beta}$	$[0,1]$
$\frac{ET}{PET_a} = \frac{\beta_w}{\beta}$	$[0,1]$
$\frac{PET_e}{PET_a} = \frac{1+\frac{1}{\beta}}{1+\frac{1}{\beta_w}}$	$\left[\frac{\beta_w}{1+\beta_w}, 1\right]$

Equation (11) clarifies the physical mechanism underlying the complementary relationship between ET and PET_a, which essentially reflects the dynamic redistribution of R_n between latent and sensible heat fluxes under varying surface wetness conditions. As the land surface dries up, ET falls below its energy-constrained upper limit, PET_e, and the excess energy not partitioned to latent heat flux is redirected to sensible heat flux, thereby driving PET_a to increase relative to PET_e (Figure 1a,b). Notably, the magnitude of PET_a's increase relative to the decrease in ET is scaled by $1/\beta_w$, a term representing the ratio of latent over sensible heat flux for the small, saturated surface. This key finding explains the observed asymmetric relationship between ET and PET_a and clarifies the physical meaning of the coefficient of proportionality (k) in the generalized linear CR framework. In essence, β_w is the source and a quantitative measure of the degree of asymmetry in the complementary relationship.

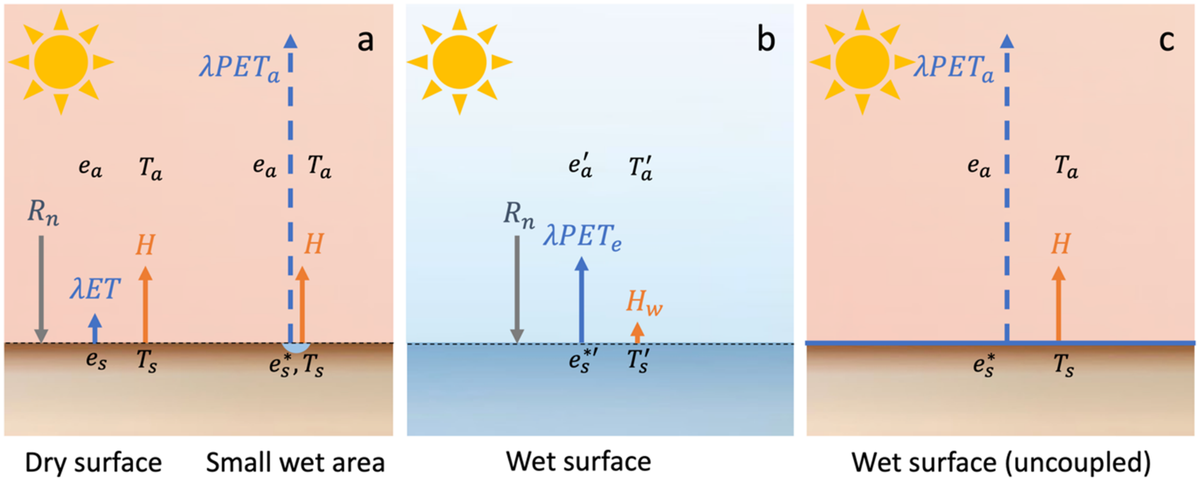

Figure 1. Schematic illustration of the relationships between actual ET and two potential ET (PET_e and PET_a) under wet and dry conditions. (**a**) In a dry environment, the available energy (R_n) is partitioned into latent heat flux (λET) and sensible heat flux (H). For an arbitrarily small wet area within this dry environment, the surface temperature (T_s), air temperature (T_a), and vapor pressure (e_a) remain the same as the surrounding dry environment. The only difference is the vapor pressure at the evaporative surface (e_s versus e_s^*). Consequently, H over the small wet area is identical to that of the surrounding dry environment, while latent heat flux (λPET_a) is substantially larger than λET, as both water and energy supply are not limiting over the small wet area. (**b**) When the entire area becomes saturated, both surface and atmospheric conditions cool down (T'_s and T'_a) and become more humid ($e_s^{*\prime}$ and e'_a) relative to the dry environment. As a result, latent heat flux (λPET_e) increases while sensible heat flux (H_w) decreases, with both constrained by R_n. (**c**) The dry surface in (**a**) is hypothetically converted to a wet surface while remaining decoupled from the atmosphere. The surface temperature (T_s) and atmospheric conditions (T_a and e_a) are identical to those in (**a**). In this hypothetical scenario, λPET_a is constrained by aerodynamic conditions, consistent with the small wet area in (**a**), with unlimited water and energy supply.

3.3. Validation of the Complementary Relationship

The Fluxnet2015 dataset, which provides meteorological measurements and observed land-atmosphere exchanges of water and energy fluxes based on the eddy covariance technique from 212 sites (>1500 site-years) around the globe [38], were used to validate the physically-based CR in Equation (11). These sites cover a wide range of climate conditions and vegetation types and were used to examine the relationship between the actual ET and potential ET, i.e., PET_e and PET_a. Data were included in this analysis for site-years where measured or high-quality gap-filled data of air temperature, surface soil temperature, sensible and latent heat fluxes were available. To reduce uncertainties in ET measurements, days with air temperature less than 5 °C or negative sensible/latent fluxes were excluded. Finally, we selected 146 Fluxnet sites with effective records of more than 90 days (see Table S1). To validate the complementary relationship for different sites and seasons, we used data from 7352 site-months, with effective records of more than 15 days for each month. For each site-month, the net radiation minus ground heat flux (R_n) was calculated as the sum of latent and sensible heat fluxes. β_w was estimated from Equation (9) subject to two constraints: $\beta_w \geq 0.24\frac{\gamma}{\Delta}$ (where Δ denotes the slope of saturation vapor pressure-temperature curve and γ is the psychrometric constant) and $\beta_w \leq \beta$, following previous studies [18,33,37]. PET_e and PET_a were estimated from Equations (6) and (8), respectively.

To illustrate the complementary relationship between ET and PET_a and the proportional relationship between ET and PET_e, Equation (11) can be scaled and re-written as

$$\frac{ET}{PET_e} = 1 + \beta_w - \beta_w \frac{PET_a}{PET_e} \tag{12}$$

$$\frac{ET}{PET_a} = (1 + \beta_w)\frac{PET_e}{PET_a} - \beta_w \tag{13}$$

Estimation of the three types of ET and their relationships are shown in Table 2 and Figure 2a–c. Based on observations from the 146 Fluxnet sites (7352 site-months), the complementary relationship between ET and PET_a and the proportional relationship between ET and PET_e across wide-ranging climate conditions are clearly evident (Figure 2d–f). The scaled ET with PET_e increases from 0 to 1 and the scaled PET_a decreases from 18 to 1 from the driest to the wettest site-months. This provides observational evidence for the complementary principle that ET and PET_a converge towards PET_e and they closely match each other ($ET = PET_e = PET_a$) under wet conditions, while ET falls below PET_e and PET_a rises above PET_e ($ET < PET_e < PET_a$) in a dry environment. As implied by Equation (12), a strong negative correlation (r = −0.86) is observed between the scaled ET and PET_a, with a low level of nonlinearity induced by variations in β_w (0.05–0.25) across the 7352 site-months (Figure 2e). The scaled ET and PET_e with PET_a in Equation (13), on the other hand, are positively correlated (r = 0.99, Figure 2f), indicating the strong positive control of energy-based PET_e on ET across a wide range of climate environments.

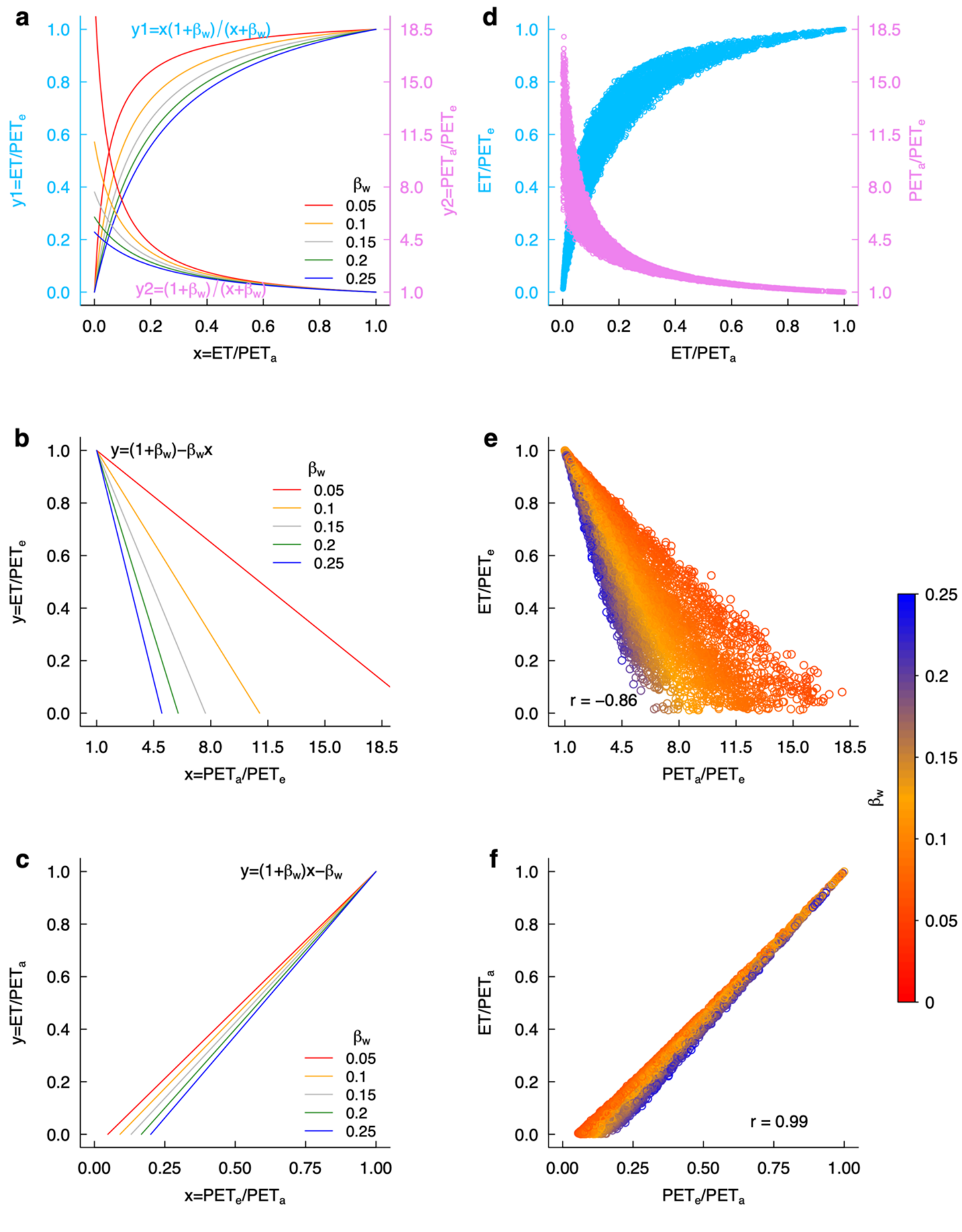

Figure 2. The complementary relationship between *ET* and *PETa* and the positive relationship between *ET* and *PETe*. (**a**–**c**) Relationships among ET, *PETe* and *PETa* with a constant value of β_w ranging from 0.05 to 0.25 at an increment of 0.05. (**d**–**f**) Relationships among monthly *ET*, *PETe* and *PETa* estimated using meteorological and flux measurements from the Fluxnet2015 dataset (146 sites and 7352 site-months in total, see Table S1). β_w is shown as variations in color for each site-month (**e**,**f**). Since β_w ranged from 0.05 to 0.25 across the 7352 site-months, the slope (β_w) would vary by a factor of 5 in Figure 2e, while for Figure 2f the range in slope ($1 + \beta_w$) varies by 19% only.

While the combined site-month patterns robustly confirm the universality of the complementary and proportional relationships, they may obscure the nuanced, climate-specific modulation of the complementary relationship. To unpack these context-dependent behaviors and validate the framework's mechanistic consistency across divergent hydroclimatic regimes, we conducted a targeted, process-level analysis focused on three Fluxnet sites representing distinct Köppen climate zones. Figure 3 confirms that the complementary relationship between ET and PET_a holds for both wet and dry climates, yet its magnitude, sensitivity to soil moisture availability, and seasonal expression exhibit pronounced climate-specific characteristics.

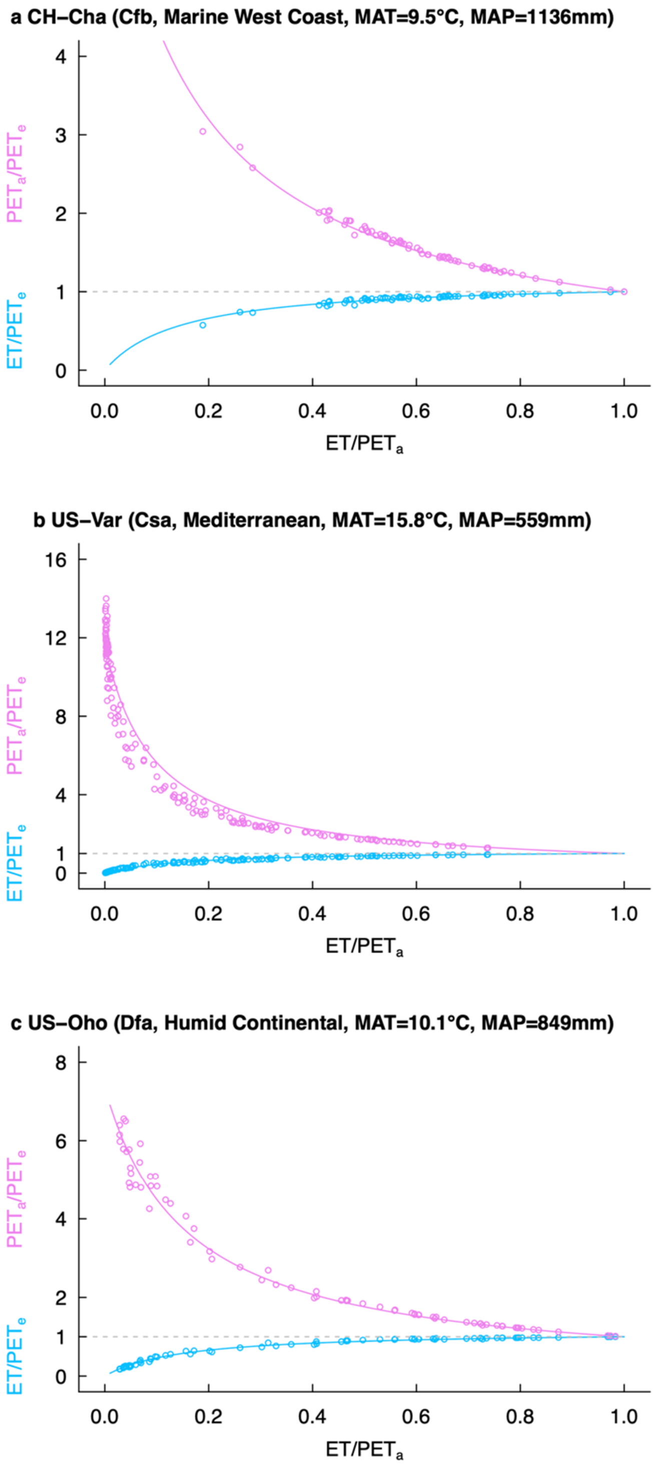

Figure 3. The complementary relationship between ET and PET_a at three Fluxnet sites. (**a**–**c**) Scaled monthly ET (ET/PET_e) and scaled monthly PET_a (PET_a/PET_e) plotted as functions of the moisture index (ET/PET_a) for the CH-Cha (**a**), US-Var (**b**), and US-Oho (**c**) sites. For each site, the Köppen climate classification, mean annual temperature (MAT), and mean annual precipitation (MAP) are shown.

At the CH-Cha site (Marine West Coast Climate), persistent maritime influence leads to high annual precipitation and relative humidity, rendering the majority of months hydrologically wet. In this energy-limited regime, the complementary relationship exhibits near-linear divergence between the scaled ET and PET_a across the moisture gradient. From the driest to the wettest months, the scaled PET_a declines gradually from 3 to 1, while the scaled ET rises concurrently from 0.57 to 1, with tight coordination across the entire moisture gradient. In contrast, the US-Var site (Mediterranean Climate) exhibits a water-limited regime marked by a pronounced seasonal imbalance between hot, dry summers and cool, wet winters. With most months characterized by soil moisture depletion, the complementary relationship is amplified to an extreme degree. During the driest months, the scaled PET_a surges to a maximum of 14, while the scaled ET drops to just 0.012. This pattern highlights the dry-climate amplification of complementarity: the relationship becomes highly sensitive to small changes in moisture availability, with ET and PET_a diverging sharply under water-limited conditions.

The US-Oho site (Humid Continental Climate) represents a transitional, energy-water co-limited regime, with distinct seasonal shifts between wet and dry periods. This duality yields a bimodal expression of the complementary relationship that integrates features of both wet and dry climates. During wet months, the scaled ET and PET_a converge to values close to 1, mirroring the complementary relationship observed at CH-Cha. In contrast, during dry months, the two variables diverge significantly: the scaled PET_a rises to 6.6 and the scaled ET drops to 0.17. This bimodal behavior demonstrates that the complementary relationship adapts dynamically to seasonal shifts in limiting factors in transitional climates, with the framework capturing both the moderation of complementarity in wet periods and its amplification in dry periods within a single site.

Collectively, these site-specific patterns show that the complementary relationship is not a static hydrometeorological phenomenon but a climate-dependent process shaped by the dominant constraints on ET. In energy-limited wet climates, complementarity is near-linear; in water-limited dry climates, it is amplified and highly nonlinear; in transitional co-limited climates, it shifts dynamically between these states seasonally. These findings validate the proposed framework, demonstrating its ability to capture the full spectrum of complementary relationship behaviors across divergent climate types.

4. Discussion

4.1. ET–PET_e–PET_a Relationship within the Land-Atmosphere System

The derivation of the CR expressed as Equation (11) confirms that the complementary relationship is essentially determined by how the available energy (R_n) is partitioned between latent and sensible heat fluxes under wet and dry conditions. Given the fundamental assumption of constant energy availability, alterations in the partitioning of latent and sensible heat fluxes manifest themselves as a complementary relationship between ET and PET_a, as the latent heat flux is directly related to ET and the sensible heat flux proportional to PET_a with the wet Bowen ratio, β_w, as the coefficient of proportionality. This physical mechanism and the core assumption are consistent with the concept of the original CR and the existing CR formulations [11,17,20–27]. However, the new physically-based CR formulation offers a clearer understanding of the nature of the complementary relationship between ET and PET_a and provides new insights into the physical basis underlying the complementary relationship.

The complementary relationship expressed in Equation (11) is highly consistent with the quantitative interactions among ET, PET_e, and PET_a derived from land-atmosphere coupling processes [33]. A notable distinction, however, lies in the definition of PET_a. According to Zhou and Yu [33], PET_a is defined as the maximum ET permissible under prevailing aerodynamic conditions for a hypothetical wet surface—decoupled from the atmosphere and supported by unlimited water and energy supply (Figure 1c). In this study, PET_a quantifies the upper limit of evaporation from a small, saturated surface that exerts no practical influence on the atmosphere, while relying on unrestricted water and energy to sustain evaporation, and its surface temperature remains identical to that of the surrounding environment. In essence, these two definitions of PET_a are conceptually consistent: both represent the maximum ET constrained solely by the prevailing aerodynamic conditions across the entire surface, with unlimited water and energy supply, regardless of the evaporative surface size. Thus, PET_a reflects the aerodynamic limit of ET, shaped by the temperature and moisture conditions of both the surface and the overlying air. It differs fundamentally from ET (constrained by water, energy, and aerodynamic conditions) and PET_e (constrained by energy and aerodynamic conditions). These distinct constraints give rise to the boundary conditions of the CR: $ET \le PET_e \le PET_a$.

From the perspective of land-atmosphere interactions [33,39], the aerodynamic conditions encapsulated by PET_a are inherently dependent on ET magnitude. ET regulates evaporative cooling effects and moisture input to the atmosphere, thereby modifying temperature and moisture dynamics of the land-atmosphere system, factors that directly shape PET_a. Specifically, the rise in PET_a relative to PET_e is an atmospheric response to reduced ET under surface water limitation, reflecting the feedback of ET on atmospheric conditions. This land-atmosphere feedback mechanism underpins the negative correlation between ET and PET_a. In contrast, ET exhibits a positive relationship with PET_e, which represents the maximum ET constrained by both energy and aerodynamic conditions that control and drive ET over land.

The theoretically sound complementary relationship also merits further interpretation of the relationship between PET_e and PET_a. Equation (11) can be re-arranged as:

$$PET_a = \left(1 + \frac{1}{\beta_w}\right) PET_e - \frac{1}{\beta_w} ET \tag{14}$$

PET_a that is related to the atmospheric conditions can be seen to depend on the energy-constrained PET_e and moisture-constrained ET. Let us consider two extreme cases: (1) where $ET = PET_e$ for saturated areas, such as the ocean and large lakes, we have the minimum of PET_a as PET_e; (2) where $ET = 0$ for surfaces of maximum dryness without supply of water vapor to the air, we have the maximum of PET_a as $\left(1 + \frac{1}{\beta_w}\right) PET_e$ and the largest difference between PET_a and PET_e, i.e., $\frac{PET_e}{\beta_w}$. This interpretation reinforces the notion that PET_a responds to water vapor supply via ET in addition to the energy constraint. The drier the air with reduced ET, the greater the difference between PET_a and PET_e.

4.2. Comparison with Previous Formulations of the Complementary Relationship

Table 1 shows that most of existing CR formulations share the same structure as Equation (11). This is because these CR formulations are developed based on the same physical principles, i.e., partitioning of the available energy shifting from latent to sensible heat flux from wet to dry conditions, from which the complementary relationship originates [11]. The physically-based CR is identical to the two empirical CRs [20,23], each involving an empirical parameter, and can be used to interpret and give meaning to these parameters. For the asymmetric CR of Brutsaert and Parlange [20], we have $b = \frac{1}{\beta_w}$, and $X_{min} = \frac{\beta_w}{1+\beta_w}$ for the rescaled CR of Crago et al. [23]. In particular, the physical meaning of X_{min} in the rescaled CR, i.e., the minimum value of $\frac{PET_e}{PET_a}$ when ET reaches zero, is consistent with our estimation of PET_e and PET_a (Table 2).

For the existing CR formulations without any parameters, or the so-called calibration-free formulations, they are essentially special cases of the physically-based CR. For example, when the air is saturated ($e_a = e_a^*$), we have $\beta_w = \frac{\gamma(T_s - T_a)}{(e_s^* - e_a^*)} = \frac{\gamma}{\Delta}$, the CR of Szilagyi [22] becomes identical to the physically-based CR. However, this special case rarely occurs, even for saturated surfaces like oceans and lakes.

The non-linear CR formulation is also similar to the physically-based CR when $\beta_w \approx 0.22$ [17]. While the non-linear CR formulation has been validated with experimental data, it is not realistic, however, under the driest conditions, i.e., $\frac{PET_e}{PET_a} < \frac{\beta_w}{1+\beta_w}$. This is because the boundary condition of the non-linear CR, i.e., $\frac{PET_e}{PET_a} \rightarrow 0$ when $ET \rightarrow 0$, is not physically sound, as PET_a cannot be infinitely large and in fact PET_a is limited by $\frac{R_n}{\beta_w}$ as ET reaches zero and H equals R_n (Table 2). To overcome this problem, the non-linear CR has been combined with the rescaled CR to develop yet another calibration-free CR [25]. However, this formulation still represents a special case without physically meaningful parameters such as β_w to account for variations in CR under different conditions.

Compared with these earlier formulations, the physically-based CR has many distinct advantages. First, PET_e and PET_a are clearly defined based on physical processes and can be estimated using observed data. Second, the basis for this new CR is physically sound and its derivation is purely based on shifts in the surface energy balance under wet and dry conditions. Third, the physical meaning of the coefficient of proportionality is clarified as the wet Bowen ratio β_w, which accounts for the degree of asymmetry in the complementary relationship across a wide range of environmental conditions. Moreover, β_w can be directly estimated from observed data without any calibration (Equation (9)). This physically-based CR can therefore be widely applied for estimating ET across different regions at various time scales. Finally, the physically-based CR clearly quantifies the complementary relationship between ET and PET_a and the positive relationship between ET and PET_e, i.e., Equations (12) and (13). This provides an enhanced understanding of the relationships among the three types of ET over land.

Differences between the physically-based CR in Equation (11) and other CR formulations essentially arise from the definition and estimation of PET_e and particularly PET_a. PET_a is commonly estimated using either pan evaporation or inferred from the Penman equation. While both approaches yield plausible PET_a estimates, neither captures the theoretical upper limit of PET_a as defined in Equation (7). In practice, the surface temperature of a small wet area (e.g., a Class A evaporation pan) is typically lower than that of the surrounding dry area (T_s), with a corresponding reduction in saturation vapor pressure. A lower PET_a based on pan evaporation measurements would increase the empirically fitted parameter k in Equation (4), bringing it closer to unity and reducing the observed asymmetry of the CR. Concurrently, the pan's Bowen ratio becomes lower than β_w, when its surface temperature is lower than T_s of the surrounding dry area. This is because β_w is positively related to T_s, as evident from rearranging Equation (9) into the following form:

$$\beta_w = \frac{\gamma}{\Delta + \frac{e_a^* - e_a}{T_s - T_a}} \tag{15}$$

where Δ is the slope of the saturation vapor pressure-temperature curve evaluated between T_s and T_a. Thus, the coefficient of proportionality, k, estimated from observations would deviate from the pan's Bowen ratio. These two only converge to and give physical meaning to the parameter k, i.e., $k = \beta_w$, when the pan's surface temperature equals that of its surrounding environment. This explains why previous CRs and their associated parameters have remained largely empirical (Table 2).

4.3. Implications for Practical Applications of the Complementary Relationship

Application of the physically-based CR for ET estimation requires values for β_w, PET_e and PET_a, all of which can be calculated using observations of meteorological variables and surface temperature data. However, the limited accessibility of surface temperature data may restrict a broader application of this method for ET estimation. To address this limitation, β_w can be approximated as

$$\beta_w = \alpha \cdot \frac{\gamma}{\Delta} \tag{16}$$

where $\frac{\gamma}{\Delta}$ can be estimated as a function of air temperature, and the coefficient α typically varies from 0.15 to 0.3, with a common approximation of $\alpha \approx 0.24$ [18,35].

While PET_e and PET_a are estimated based on energy balance and aerodynamic principles, respectively, they can also be derived using modified versions of the Penman equation with introduction of an adjustment parameter k' [18]. For a saturated evaporative surface, the original Penman equation can be used to estimate both PET_e and PET_a, i.e., $ET = PET_e = PET_a$ [32]. However, direct application of the Penman equation tends to overestimate PET_e [37,40,41] while underestimating PET_a in a dry environment [18]. This dual bias arises from two key factors: (1) PET_e is defined for a large, saturated surface (Figure 1b), so using meteorological variables corresponding to dry surface conditions inflates its aerodynamic component; (2) PET_a applies to a small, saturated surface (Figure 1a), but the Penman equation does not account for energy transfer from the surrounding dry environment, leading to underestimated energy supply for evaporation. These issues can be resolved with the adjustment parameter k', yielding the modified Penman equations for PET_e and PET_a:

$$\lambda PET_e = \frac{\Delta R_n + k' \frac{\rho c_p (e_a^* - e_a)}{r_a}}{\Delta + \gamma} \tag{17}$$

$$\lambda PET_a = \frac{\Delta R_n / k' + \frac{\rho c_p (e_a^* - e_a)}{r_a}}{\Delta + \gamma} \tag{18}$$

where e_a^* is the saturation vapor pressure at air temperature (Pa), and $e_a^* - e_a$ is the vapor pressure deficit. The parameter k' can be determined by equating PET_e from Equations (6) and (17), and k' so determined can be used to compute PET_a via Equation (18). This approach enables estimation of β_w, PET_e and PET_a using only routine meteorological variables, thereby expanding the practical applications of the physically-based CR for ET estimation.

5. Conclusions

In this study, we demonstrate that the complementary relationship naturally emerges from surface energy balance, achieved by estimating PET_e and PET_a using energy balance and aerodynamic principles, respectively. The complementary relationship between ET and PET_a fundamentally originates from the partitioning of available energy between latent and sensible heat fluxes, with ET directly related to the latent heat flux and PET_a proportional to the sensible heat flux. Furthermore, the complementary relationship is reinforced by the atmospheric response, characterized by PET_a, to ET dynamics as surface moisture changes. In contrast, ET is positively related to PET_e, which represents the atmospheric evaporative demand that controls and drives ET over land. The wet Bowen ratio (β_w), defined as the Bowen ratio when the surface becomes saturated, quantifies the asymmetry of the complementary relationship. By clarifying the quantitative relationship between the three types of ET, this study advances mechanistic understanding of the complementary relationship and would promote and facilitate practical application of the complementary relationship for ET estimation across different regions and time scales.

Supplementary Materials

The additional data and information can be downloaded at: https://media.sciltp.com/articles/others/2601291058148163/HWR-25110094-Author-SI-of-CR-1.pdf. Table S1. List of the 146 Fluxnet sites used in this study.

Author Contributions

S.Z. conceived the study, performed the data analysis, and wrote the initial manuscript. B.Y. provided critical revisions and edits. All authors have read and agreed to the published version of the manuscript.

Funding

We acknowledge all the principal investigators who contributed data to the Fluxnet2015 dataset (Table S1). This work was supported by the National Natural Science Foundation of China (42471108) and the National Key Research and Development Program of China (2022YFF0801303).

Data Availability Statement

The Fluxnet2015 dataset is publicly available from https://fluxnet.org/data/fluxnet2015-dataset/ (accessed on 27 January 2026).

Conflicts of Interest

The authors declare that they have no conflict of interest.

Use of AI and AI-Assisted Technologies

No AI tools were utilized for this paper.

References

1. Katul, G.G.; Oren, R.; Manzoni, S.; et al. Evapotranspiration: A Process Driving Mass Transport and Energy Exchange in the Soil-Plant-Atmosphere-Climate System. *Rev. Geophys.* **2012**, *50*. https://doi.org/10.1029/2011RG000366.
2. Fisher, J.B.; Melton, F.; Middleton, E.; et al. The Future of Evapotranspiration: Global Requirements for Ecosystem Functioning, Carbon and Climate Feedbacks, Agricultural Management, and Water Resources. *Water Resour. Res.* **2017**, *53*, 2618–2626. https://doi.org/10.1002/2016WR020175.
3. Yang, Y.; Roderick, M.L.; Guo, H.; et al. Evapotranspiration on a Greening Earth. *Nat. Rev. Earth Environ.* **2023**, *4*, 626–641. https://doi.org/10.1038/s43017-023-00464-3.
4. Gu, B.; Zhou, S.; Yu, B.; et al. Multifaceted Changes in Water Availability with a Warmer Climate. *npj Clim. Atmos. Sci.* **2025**, *8*, 31. https://doi.org/10.1038/s41612-025-00913-4.
5. Wang, K.; Dickinson, R.E. A Review of Global Terrestrial Evapotranspiration: Observation, Modeling, Climatology, and Climatic Variability. *Rev. Geophys.* **2012**, *50*. https://doi.org/10.1029/2011RG000373.
6. Zhang, Y.; Kong, D.; Gan, R.; et al. Coupled Estimation of 500 m and 8-Day Resolution Global Evapotranspiration and Gross Primary Production in 2002–2017. *Remote Sens. Environ.* **2019**, *222*, 165–182. https://doi.org/10.1016/j.rse.2018.12.031.
7. Miralles, D.G.; Bonte, O.; Koppa, A.; et al. GLEAM4: Global Land Evaporation and Soil Moisture Dataset at 0.1 Resolution from 1980 to near Present. *Sci Data* **2025**, *12*, 416. https://doi.org/10.1038/s41597-025-04610-y.
8. Zhang, K.; Kimball, J.S.; Running, S.W. A Review of Remote Sensing Based Actual Evapotranspiration Estimation. *WIREs Water* **2016**, *3*, 834–853. https://doi.org/10.1002/wat2.1168.
9. Zhou, S.; Keenan, T.F.; Williams, A.P.; et al. Large Divergence in Tropical Hydrological Projections Caused by Model Spread in Vegetation Responses to Elevated CO_2. *Earth's Future* **2022**, *10*, e2021EF002457. https://doi.org/10.1029/2021EF002457.
10. Raoult, N.; Douglas, N.; MacBean, N.; et al. Parameter Estimation in Land Surface Models: Challenges and Opportunities With Data Assimilation and Machine Learning. *J. Adv. Model. Earth Syst.* **2025**, *17*, e2024MS004733. https://doi.org/10.1029/2024MS004733.

11. Bouchet, R.J. Evapotranspiration Reelle, Evapotranspiration Potentielle, et Production Agricole. *Ann. Agron.* **1963**, *14*, 743–824.
12. Morton, F.I. Operational Estimates of Areal Evapotranspiration and Their Significance to the Science and Practice of Hydrology. *J. Hydrol.* **1983**, *66*, 1–76. https://doi.org/10.1016/0022-1694(83)90177-4.
13. Han, S.; Tian, F. A Review of the Complementary Principle of Evaporation: From the Original Linear Relationship to Generalized Nonlinear Functions. *Hydrol. Earth Syst. Sci.* **2020**, *24*, 2269–2285. https://doi.org/10.5194/hess-24-2269-2020.
14. Zhang, L.; Brutsaert, W. Blending the Evaporation Precipitation Ratio With the Complementary Principle Function for the Prediction of Evaporation. *Water Resour. Res.* **2021**, *57*, e2021WR029729. https://doi.org/10.1029/2021WR029729.
15. Ma, N.; Szilagyi, J.; Zhang, Y. Calibration-Free Complementary Relationship Estimates Terrestrial Evapotranspiration Globally. *Water Resour. Res.* **2021**, *57*, e2021WR029691. https://doi.org/10.1029/2021WR029691.
16. Ma, N.; Szilagyi, J.; Zhang, Y. Hydrological Responses to Warming: Insights From Centennial-Scale Terrestrial Evapotranspiration Estimates. *Water Resour. Res.* **2025**, *61*, e2025WR041001. https://doi.org/10.1029/2025WR041001.
17. Brutsaert, W. A Generalized Complementary Principle with Physical Constraints for Land-surface Evaporation. *Water Resour. Res.* **2015**, *51*, 8087–8093. https://doi.org/10.1002/2015WR017720.
18. Zhou, S.; Yu, B. Physical Basis of the Potential Evapotranspiration and Its Estimation over Land. *J. Hydrol.* **2024**, *641*, 131825. https://doi.org/10.1016/j.jhydrol.2024.131825.
19. Kahler, D.M.; Brutsaert, W. Complementary Relationship between Daily Evaporation in the Environment and Pan Evaporation: Daily and Pan Evaporation. *Water Resour. Res.* **2006**, *42*. https://doi.org/10.1029/2005WR004541.
20. Brutsaert, W.; Parlange, M.B. Hydrologic Cycle Explains the Evaporation Paradox. *Nature* **1998**, *396*, 30. https://doi.org/10.1038/23845.
21. Granger, R.J. A Complementary Relationship Approach for Evaporation from Nonsaturated Surfaces. *J. Hydrol.* **1989**, *111*, 31–38. https://doi.org/10.1016/0022-1694(89)90250-3.
22. Szilagyi, J. On the Inherent Asymmetric Nature of the Complementary Relationship of Evaporation. *Geophys. Res. Lett.* **2007**, *34*, L02405. https://doi.org/10.1029/2006GL028708.
23. Crago, R.; Szilagyi, J.; Qualls, R.; et al. Rescaling the Complementary Relationship for Land Surface Evaporation. *Water Resour. Res.* **2016**, *52*, 8461–8471. https://doi.org/10.1002/2016WR019753.
24. Aminzadeh, M.; Roderick, M.L.; Or, D. A Generalized Complementary Relationship between Actual and Potential Evaporation Defined by a Reference Surface Temperature. *Water Resour. Res.* **2016**, *52*, 385–406. https://doi.org/10.1002/2015WR017969.
25. Szilagyi, J.; Crago, R.; Qualls, R. A Calibration-Free Formulation of the Complementary Relationship of Evaporation for Continental-Scale Hydrology. *J. Geophys. Res. Atmos.* **2017**, *122*, 264–278. https://doi.org/10.1002/2016JD025611.
26. Szilagyi, J.; Ma, N.; Crago, R.D.; et al. Power-Function Expansion of the Polynomial Complementary Relationship of Evaporation. *Water Resour. Res.* **2022**, *58*, e2022WR033095. https://doi.org/10.1029/2022WR033095.
27. Tu, Z.; Yang, Y.; Roderick, M.L.; et al. Potential Evaporation and the Complementary Relationship. *Water Resour. Res.* **2023**, *59*, e2022WR033763. https://doi.org/10.1029/2022WR033763.
28. Zhang, L.; Cheng, L.; Brutsaert, W. Estimation of Land Surface Evaporation Using a Generalized Nonlinear Complementary Relationship. *J. Geophys. Res. Atmos.* **2017**, *122*, 1475–1487. https://doi.org/10.1002/2016JD025936.
29. Brutsaert, W.; Cheng, L.; Zhang, L. Spatial Distribution of Global Landscape Evaporation in the Early Twenty-First Century by Means of a Generalized Complementary Approach. *J. Hydrometeorol.* **2020**, *21*, 287–298. https://doi.org/10.1175/JHM-D-19-0208.1.
30. Tu, Z.; Yang, Y.; Ruan, F.; et al. Global Terrestrial Evaporation from Physically-Based, Calibration-Free Complementary Relationship. *J. Hydrol.* **2025**, *660*, 133382. https://doi.org/10.1016/j.jhydrol.2025.133382.
31. Priestley, C.H.B.; Taylor, R.J. On the Assessment of Surface Heat Flux and Evaporation Using Large-Scale Parameters. *Mon. Wea. Rev.* **1972**, *100*, 81–92.
32. Penman, H.L. Natural Evaporation from Open Water, Bare Soil and Grass. *Proc. R. Soc. London. Ser. A Math. Phys. Sci.* **1948**, *192*, 120–145.
33. Zhou, S.; Yu, B. Neglecting Land–Atmosphere Feedbacks Overestimates Climate-Driven Increases in Evapotranspiration. *Nat. Clim. Chang.* **2025**, *15*, 1099–1106. https://doi.org/10.1038/s41558-025-02428-5.
34. Szilagyi, J. On the Thermodynamic Foundations of the Complementary Relationship of Evaporation. *J. Hydrol.* **2021**, *593*, 125916. https://doi.org/10.1016/j.jhydrol.2020.125916.
35. Yang, Y.; Roderick, M.L. Radiation, Surface Temperature and Evaporation over Wet Surfaces. *Q. J. R. Meteorol. Soc.* **2019**, *145*, 1118–1129. https://doi.org/10.1002/qj.3481.
36. Kim, Y.; Garcia, M.; Johnson, M.S. Land-Atmosphere Coupling Constrains Increases to Potential Evaporation in a Warming Climate: Implications at Local and Global Scales. *Earth's Future* **2023**, *11*, e2022EF002886. https://doi.org/10.1029/2022EF002886.

37. Zhou, S.; Yu, B. Reconciling the Discrepancy in Projected Global Dryland Expansion in a Warming World. *Glob. Chang. Biol.* **2025**, *31*, e70102. https://doi.org/10.1111/gcb.70102.
38. Pastorello, G. The FLUXNET2015 Dataset and the ONEFlux Processing Pipeline for Eddy Covariance Data. *Sci. Data* **2020**, *7*, 225.
39. Zhou, S.; Williams, A.P.; Berg, A.M.; et al. Land–Atmosphere Feedbacks Exacerbate Concurrent Soil Drought and Atmospheric Aridity. *Proc. Natl. Acad. Sci. USA* **2019**, *116*, 18848–18853. https://doi.org/10.1073/pnas.1904955116.
40. Milly, P.C.D.; Dunne, K.A. A Hydrologic Drying Bias in Water-Resource Impact Analyses of Anthropogenic Climate Change. *JAWRA J. Am. Water Resour. Assoc.* **2017**, *53*, 822–838. https://doi.org/10.1111/1752-1688.12538.
41. Milly, P.C.D.; Dunne, K.A. Potential Evapotranspiration and Continental Drying. *Nat. Clim. Chang.* **2016**, *6*, 946–949. https://doi.org/10.1038/nclimate3046.